Gunjan Pahuja, T. N. Nagabhushan and Bhanu Prasad*

Early Detection of Parkinson's Disease by Using SPECT Imaging and Biomarkers

https://doi.org/10.1515/jisys-2018-0261
Received June 17, 2018; previously published online March 27, 2019.

Abstract: Precise and timely diagnosis of Parkinson's disease is important to control its progression among subjects. Currently, a neuroimaging technique called dopaminergic imaging that uses single photon emission computed tomography (SPECT) with ^{123}I-Ioflupane is popular among clinicians for detecting Parkinson's disease in early stages. Unlike other studies, which consider only low-level features like gray matter, white matter, or cerebrospinal fluid, this study explores the non-linear relation between different biomarkers (SPECT + biological) using deep learning and multivariate logistic regression. Striatal binding ratios are obtained using ^{123}I-Ioflupane SPECT scans from four brain regions which are further integrated with five biological biomarkers to increase the diagnostic accuracy. Experimental results indicate that this investigated approach can differentiate subjects with 100% accuracy. The obtained results outperform the ones reported in the literature. Furthermore, logistic regression model has been developed for estimating the Parkinson's disease onset probability. Such models may aid clinicians in diagnosing this disease.

Keywords: Parkinson's disease (PD), striatal binding ratio (SBR), biological biomarkers, multivariate logistic regression (MLR), risk prediction, deep learning.

1 Introduction

According to Booij et al. [3], Parkinson's disease (PD) is a progressive neurodegenerative disorder caused by loss of dopaminergic neurons in substantia nigra of the midbrain which further results in loss of dopamine transporters in striatum. Till date, there is no blood/lab test for identifying PD and its progression. If PD is detected in the advanced stages, its speed of progression becomes difficult to contain. Thus, early and accurate diagnosis of this disease is necessary for better management and to evade unnecessary medical examinations involving financial expenses and other risks [5].

Hence, the focus of this study is to investigate the non-linear relation between imaging and biological biomarkers so that the accuracy of PD detection would increase. Another objective of this study is to create a logistic regression model for the risk estimation of this disorder. To fulfill our objectives, we showcased a different supervised classification approach based on deep learning [30] and statistical approach based on multivariate logistic regression (MLR) [23] to build the classification as well as risk estimation/prediction model. For this study, the dataset, in terms of matched biomarkers, has been collected from Parkinson's Progressive Markers Initiative (PPMI). Matched biomarkers mean that those subjects have been considered for which both biomarkers, i.e. single photon emission computed tomography (SPECT) as well as biological features, were available. The obtained results clearly indicate the potential of this study over the existing studies.

***Corresponding author: Bhanu Prasad,** Department of Computer and Information Sciences, Florida A&M University, Tallahassee, FL 32307, USA, e-mail: bhanu.prasad@famu.edu
Gunjan Pahuja: Department of Computer Science and Engineering, JSS Academy of Technical Education, Noida 201301, India; and Dr. A. P. J. Abdul Kalam Technical University, Lucknow, India
T. N. Nagabhushan: Department of Information Science and Engineering, Sri Jayachamarajendra College of Engineering, Mysuru 570006, India

The rest of the paper is outlined as follows. Section 2 describes the motivation behind this study and represents the review of literature on this proposed approach. Section 3 discusses the methods and materials used to model the diagnostic tool based on deep learning and MLR. Section 4 provides the results, and, finally, Section 5 concludes the work along with future prospects.

2 Review of Literature

Diagnosing the PD at its early stage is important. Therefore, nowadays, SPECT with ^{123}I-Ioflupane (DaTSCAN) is being widely used to identify PD-affected persons by illustrating the presynaptic dopaminergic deficiency in striatum, i.e. left caudate (LC), right caudate (RC), left putamen (LP), and right putamen (RP), even in the starting stages of this disease [3, 23, 26, 27, 33]. Striatal binding ratio (SBR), calculated from SPECT, is becoming a valuable tool for diagnosing this disease [23]. In order to accurately detect PD, researchers are focusing on identifying the biomarkers that can support clinicians in diagnosing PD in a stage where therapy is likely to be most effective [4, 25, 28]. Various biological biomarkers for identifying PD symptoms are plasma, serum, urine, cerebrospinal fluid (CSF), and ribonucleic acid (RNA) [21]. Both SBR values and biological biomarkers are contributing towards PD diagnosis. Therefore, we proposed a different approach to classify the subjects using deep learning and MLR by integrating both types of features (SBR values from SPECT and biological biomarkers). In addition, the diagnostic/indicative tools, which are based on deep learning and MLR, are being widely used for PD diagnosis, as these tools can assist clinicians in the early detection, management, and progression tracking of the neurodegenerative diseases [23, 30]. Deep learning has been increasingly used in the fields of speech, image, video, text mining, etc., due to its strong ability to represent the features [12, 13]. Motivated by the work done so far, we also tried to take advantage of deep learning to improve the classification accuracy for PD diagnosis. To realize the latent representation from neuroimaging and biological biomarkers, 'stacked auto-encoder' [30] has been used. Similar kind of deep learning-based architectures have also shown their efficacy in detecting other neurodegenerative diseases like Alzheimer's [30]. Zhang [35] presented a smartphone based on stacked auto-encoder, which can diagnose PD using the voice of the subjects. Though the research conducted by Zhang was very motivating and has potentials for diagnosing PD, further advancements are required due to stability and robustness issues of telediagnosis systems. Recent studies conducted by Martinez-Murcia et al. [16] and Kadam and Jadhave [9] indicated the potential of deep learning-based architectures in diagnosing PD accurately. These research studies highlighted the accuracy of over 93% using DaTSCAN and over 90% using publically available voice dataset respectively.

Studies available in the literature also support the use of ^{123}I-Ioflupane in depicting the progression of dopamine degeneration in PD [14, 26]. Martinez-Murcia et al. [14] proposed a fully automated system for diagnosing PD using ^{123}I-ioflupane images and observed an accuracy of 97.4% using leave-one-out cross-validation (LOOCV) method. Though promising results have been observed by these researchers, but with higher computational cost. Segovia et al. [26] did the classification of the subjects by extracting the voxels from the corresponding striatum and then performed data analysis using partial least squares method. An accuracy of 94% has been observed using support vector machine (SVM) classifier. Kish et al. [10] examined the loss of dopamine in striatum in eight idiopathic PD patients and observed that there is complete depletion of dopamine in putamen and caudate in affected persons as compared to normal subjects. Although these researchers provided detailed information on neurosurgical strategy of autografting in patients with PD, the sample size taken for analysis was very small. Takaya et al. [31] performed image-based classification for detecting PD using an integration of dopamine transporter and SPECT images. Total diagnostic accuracy of 86.1% was observed using LOOCV method. Martinez-Murcia et al. [15] achieved 95.5% accuracy and 96.2% sensitivity for classifying PD affected and non-affected subjects by employing convolution neural networks (CNNs) using SPECT images. However, the existing studies have limitations and they include the following:

(1) The dataset used in the studies was of limited size. In some studies, it is limited to 10 patients or healthy subjects.
(2) The studies mandate the usage of feature subset selection methods, which lead to information loss. This impacts the accuracy.
(3) Correlation information is missing among biomarkers employed during the studies.

Thus, the contributions of this study are the following:

(1) Usage of only four SBR features and five biological biomarkers for developing the classification model for PD identification, without compromising the accuracy. SBR values are computed from four striatal regions, namely, LC, RC, LP, and RP, using automated algorithms [36] which are publicly available at PPMI. The five most affecting biological biomarkers are also available on PPMI. PPMI is one of the largest databases in the public domain which provide data to researchers and scientists for further studies on PD. In addition, PPMI database involves subjects from different countries, thus making the dataset more robust. The performance of softmax classifier has been evaluated on the integrated dataset (by considering different possible combinations), and it has been observed that the obtained accuracy is higher than the accuracy available in the literature [15, 23].

(2) To the extent of our knowledge, this is the first instance of jointly using the deep neural network and logistic regression approaches for classification/prediction modeling using neuroimaging (SPECT) and biological biomarkers. Further, the matched dataset taken is quite significant (532 subjects – 384 PD and 148 normal) resulting in higher accuracy.

3 Methods and Materials

In this research, SBR values from the four regions (LC, RC, LP, and RP) have been considered, and these values were calculated from DaTSCAN SPECT images and are openly available at http://www.ppmi-info.org/data. In addition to these features, five biological biomarkers have also been factored to enhance the accuracy of the proposed method. The schematic diagram of the proposed method is shown in Figure 1.

3.1 Database Details

The database was downloaded on 20th of December 2017. Although SBR values from a large number of subjects were available, we considered only 532 subjects (384 PD and 148 normal subjects) because of the availability of other matched biomarkers. The demographic details of the subjects used in this study, along with the SBR values and biological biomarkers, are depicted in Table 1. The steps outlined by the Imaging

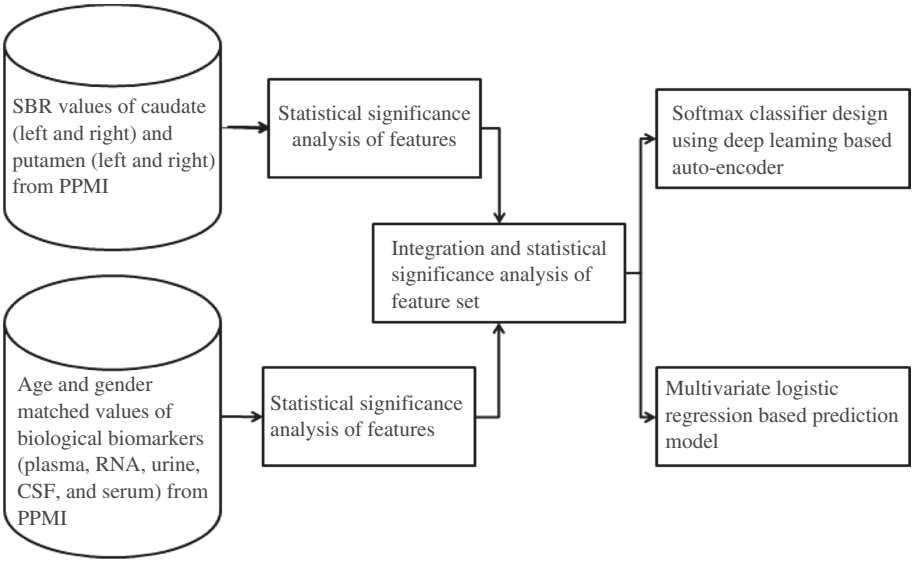

Figure 1: Steps of the Analysis Carried Out for Classification/Prediction of PD Subjects.

Table 1: Details of the Subjects (Mean ± Standard Deviation) Used in this Study.

Subjects	Number of persons	Sex (M/F)	Age (range)	Striatal binding ratio (SBR)				Biological biomarkers				
				Left caudate	Right caudate	Left putamen	Right putamen	CSF	RNA	Plasma	Serum	Urine
Control	148	98/50	31–84	2.98 ± 0.61	2.92 ± 0.59	2.11 ± 0.55	2.13 ± 0.56	14.48 ± 3.11	0.14 ± 0.02	4.31 ± 0.84	3.79 ± 1.09	13.78 ± 2.88
PD	384	250/134	33–84	1.99 ± 0.59	1.99 ± 0.60	0.81 ± 0.36	0.84 ± 0.36	14.03 ± 2.58	0.14 ± 0.01	4.23 ± 0.79	3.70 ± 0.94	13.43 ± 2.92

Core of PPMI for calculating SBR from a definite region of DaTSCAN are described at http://www.ppmi-info.org/about-ppmi/who-we-are/study-cores/. After the collection of raw projection data, Central SPECT Core lab performed the reconstruction, noise correction, and data analysis with a standard region of interest template on caudate, putamen, and occipital lobe regions. The region count densities for LC, RC, LP, and RP were extracted. The SBR of a target region is obtained by dividing the density of target region count with reference region count, i.e. SBR of a target region $=$ (Density of target region count)/(Density of reference region count).

3.2 Identification of Statistically Significant Features from Independent and Integrated Dataset

In this study, for assessing the statistical significance ($p < 0.05$; where p is the probability value) of SBR-based features and biological biomarkers, Minitab statistical tool, available at http://www.minitab.com/en-us/downloads, was used. To visualize the SBR features and biological features of normal and PD subjects' population, histograms (Figure 2A–F) and box plots (Figure 2G–L) have been plotted. Box plots are used to demonstrate the distribution shape, central value, and the variations of a dataset. The central line in the box plot signifies the median, and the edges of the box denote the 25th (lower quartile) and 75th (upper quartile) percentiles of the data. The variations outside the 25th and 75th percentiles (which are not considered as outliers) are plotted with the help of the extended whiskers. From the box plots (Figure 2G–L) it can be observed that the SBR values LC, RC, LP, and RP of PD subjects is significantly less when compared to the healthy subjects. The histogram plots illustrate the extent of overlapping of distribution between PD and the normal subjects' population. If the overlapping between the plots is more, it is more difficult to classify the subjects. The application of diagnostic tools, based on statistical theory and deep learning algorithms, come into play as both these approaches have the capability to integrate the characteristics across the distributed populations having high dimensional feature set. The flow of work carried out in this study has been shown in Figure 1. Since we used integrated dataset from different modalities along with class labels, it is required to check the significance of the features. For this purpose, first, we checked the significance of the features individually and then by feature combinations with the boundary as $p < 0.05$. Further, we checked whether PD is dependent on age and gender. This was done by checking the value of p, which was greater than 0.05 ($p > 0.05$). Hence, it was inferred that PD is not dependent on age and gender.

3.3 Classification/Prediction Modeling to Categorize the Subjects Using Deep Learning and MLR

Deep learning and statistical modeling methods are widely used in biomedicine for model creation, and they facilitate the clinicians in better decision making [1, 6, 23, 30]. The goal of deep learning algorithms is to extract information from raw data and represent it in the form of a model which can be used for interpreting other data that has not been modeled yet [7]. On the other hand, statistical modeling deals with the formalization of relationships between variables in the form of mathematical equations. Deep-learning techniques have been successfully applied in various fields, and the obtained results have dominated the traditional methods which are based on artificial intelligence [7, 17, 20, 22]. Deep learning techniques have been primarily categorized as CNNs and auto-encoder (AE). CNNs are biologically inspired by animal visual cortex and consist of 'convolutional layer,' 'pooling layer,' and 'fully connected layer' [6]. However, overfitting may happen due to complicated and fully connected layers in CNN. On the other hand, the aim of AE is to learn a representation for a set of data to reduce the dimensionality [30]. In addition, it is easier to create AE model and further train it. AE has been successfully implemented for content-based image retrieval [11], image super-resolution [34], and prediction and classification [17, 20, 29]. Therefore, in this study, we

used the stacked AE and softmax classifier for differentiating PD patients from the normal population. For statistical/prediction modeling, MLR has been used. Logistic regression not only calculates the class-conditional probabilities but also yields estimated probabilities, which give more meaningful information to clinicians.

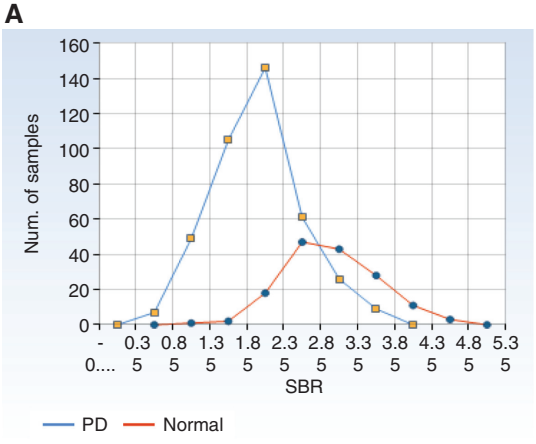

Histogram- SBR of left caudate for normal and PD subjects

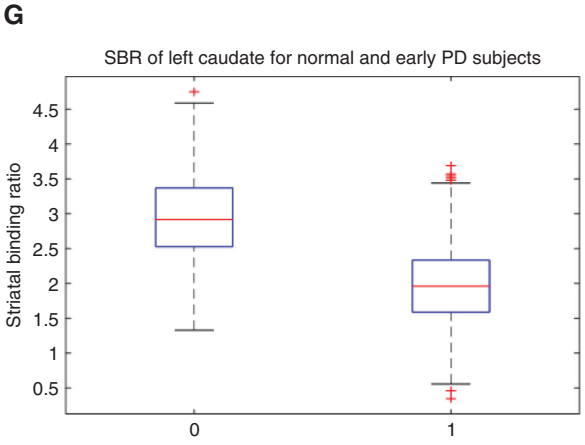

Box plot-SBR of left caudate for normal and PD subjects

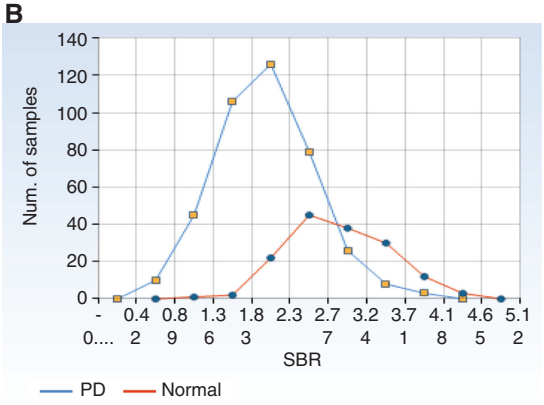

Histogram: SBR of right caudate for normal and PD subjects

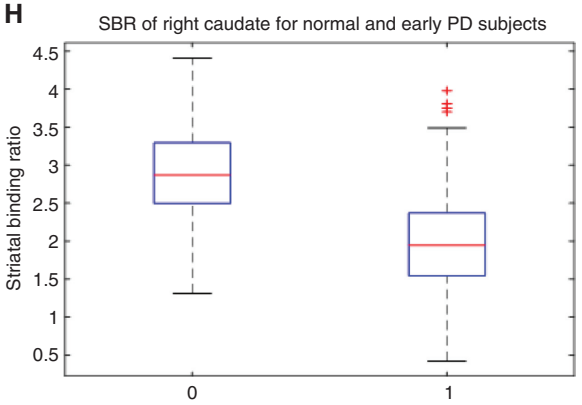

Box plot-SBR of right caudate for normal and PD subjects

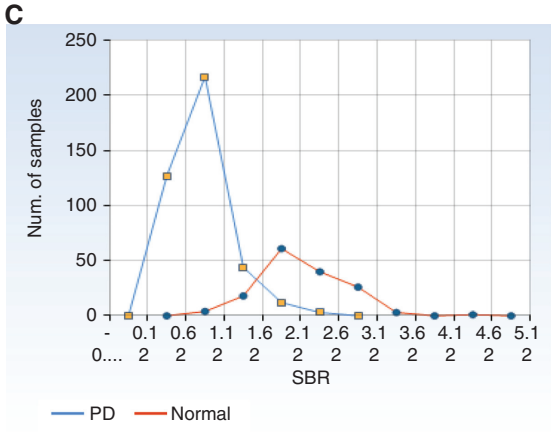

Histogram: SBR of left putamen for normal and PD subjects

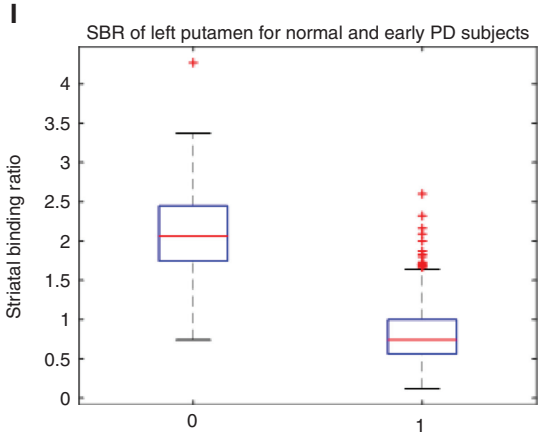

Box plot-SBR of left putamen for normal and PD subjects

Figure 2: Histogram and Box Plots of SBR Values for Left Caudate (A, G), Right Caudate (B, H), Left Putamen (C, I), Right Putamen (D, J), CSF Biomarker (E, K), and Urine Biomarker (F, L) for PD and Normal Subjects Population.

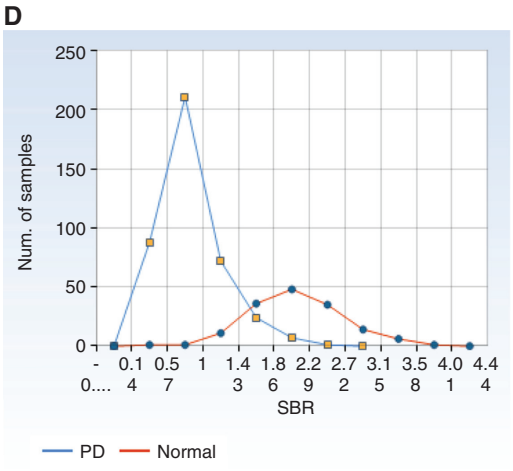

Histogram: SBR of right putamen for normal and PD subjects

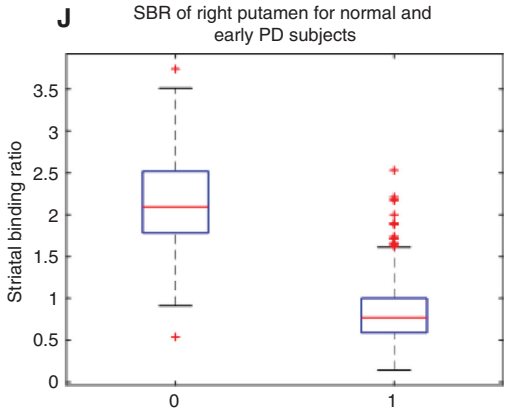

Box plot-SBR of right putamen for normal and PD subjects

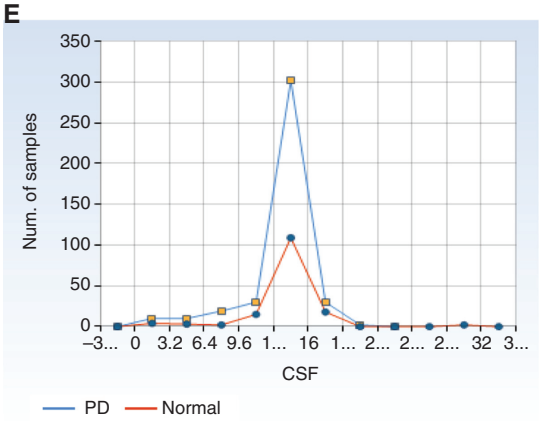

Histogram: CSF biomarker for normal and PD subjects

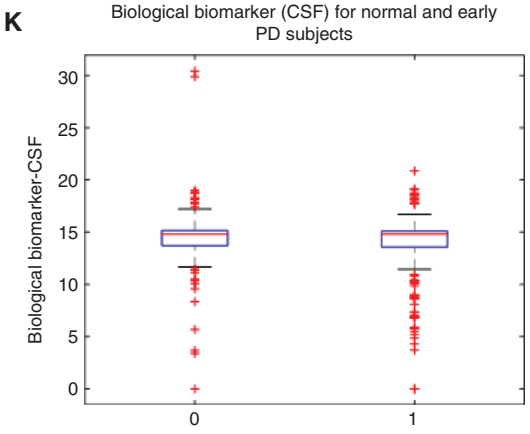

Box plot-CSF biomarker for normal and PD subjects

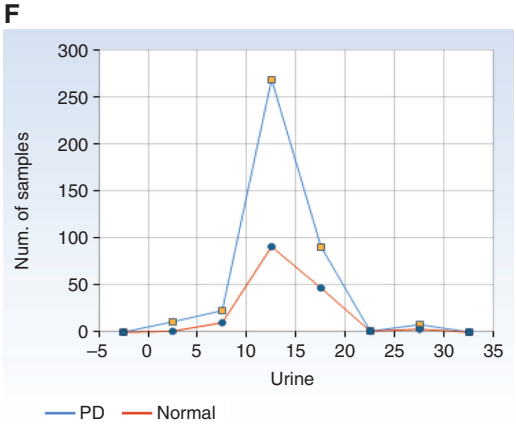

Histogram: urine biomarker for normal and PD subjects

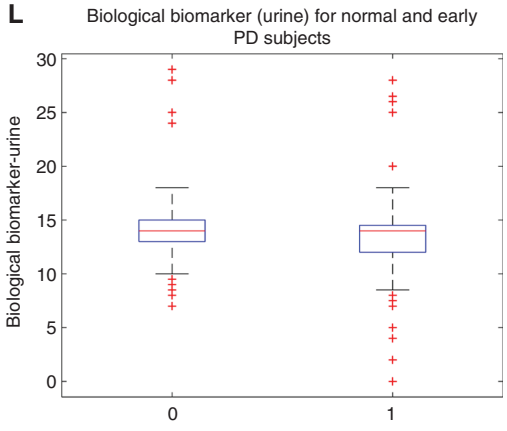

Box plot-urine or normal and PD subjects

Figure 2 (continued)

3.3.1 Stacked AE-Based Classification

An 'AE' is defined as a feed-forward neural network comprising an encoder and decoder (Figure 3). Similar to multilayer perceptron, it also contains an input layer, single or multiple hidden layers, and an output layer. The output layer consists of the same number of nodes as the input layer [24]. The study conducted by Bengio

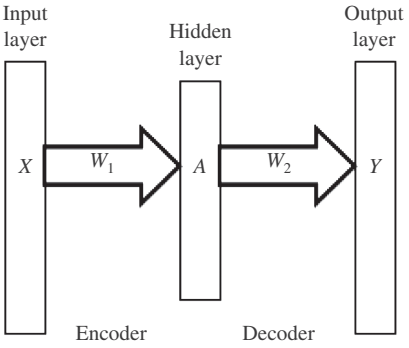

Figure 3: Auto-encoder Structure.
X, *Y*, *A*, W_1, and W_2 Represent an Input Vector, Output Vector, Output of the Hidden Layer, and Weight Matrix of the Encoder and Decoder, respectively.

[2] indicates that the deep architectures are helpful not only to find the non-linear relationships but also to find complex patterns in the dataset.

Since the dataset being used in this study was also non-linear, sparse auto-encoder (SAE) [30] has been considered for representing the features. In SAE, the non-linear relation can be obtained by using more number of hidden layer units as compared to the input dimensions. If sparsity is imposed on the hidden units while training the data, then AE can acquire useful and interesting patterns from the input data which is helpful in pre-training for classification tasks.

Let the dataset representation be $x_i \in R^d,\ i = 1,\ 2, \ldots,\ n$, where n is the total number of observations, and d is the number of features which is 9. Let N_I and N_H represent the number of input and hidden units, respectively. Given an input vector $\in R^{N_I}$, an AE maps it to a compressed/latent representation Y, by using the following deterministic mapping [30]:

$$A = f(W_1 X + b_1) \tag{1}$$

where W_1 is the weight matrix and $W_1 \in R^{N_I * N_H}$, b_1 is the bias vector and $b_1 \in R^{N_H}$, and f is an activation function which is a logistic sigmoid function, i.e.

$$f(z) = 1/(1 + \exp(-z)) \tag{2}$$

After that, the decoder stage maps A ($A \in R^{N_H}$) to the reconstruction Y ($Y \in R^{N_I}$) of the same shape as X, by using another deterministic mapping:

$$Y = f'(W_2 A + b_2) \approx X \tag{3}$$

where f', W_2, and b_2 are the activation function, weight, and bias, respectively, for the decoder, which may vary based on f, W_1,, and b_1 for the encoder. The core function of an 'AE' is error minimization between input vector X and output vector Y, which can be expressed as

$$F(W_1, W_2, b_1, b_2) = \frac{1}{2}||Y - X||^2 \tag{4}$$

From Equations (1) and (2), Y can be written as

$$Y = h(X|W_1, W_2, b_1, b_2) \tag{5}$$

Equation (4) can be rewritten as

$$\mathrm{F}\ (W_1\ , W_2\ ,\ b_1\ ,\ b_2)\ = \frac{1}{2}||h(X|(W_1, W_2\ ,\ b_1\ ,\ b_2) - X||^2 \tag{6}$$

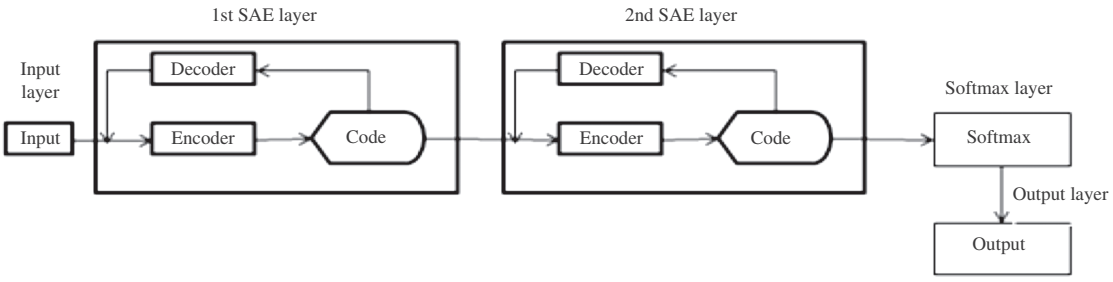

Figure 4: Structure of Deep Neural Network.

where X is generally averaged over some of the input training set.

To improve the classification accuracy in diagnosing PD, we have optimized the assumed deep architecture in a supervised manner. For this purpose, another layer called 'softmax classifier' has been stacked on SAE (Figure 4) as the last layer to classify the subjects [9, 29]. Since softmax classifier gives more intuitive output that is easy to interpret than SVM (SVM provides uncalibrated and perhaps difficult to interpret output), we have considered this classifier in this study.

Softmax classifier uses 'softmax' as the activation function, i.e. $f_j(z) = \frac{e^{z_j}}{\sum_k e^{z_k}}$. This function captures a random vector with real value scores in z and minimizes it to a vector of values in the range (0, 1), and aggregating to 1 [9].

3.3.2 Prediction Modeling through MLR

To develop the prediction model for estimating PD risk, MLR method has been widely used [23, 32]. Since PD detection is a dichotomous classification problem, binary logistic regression method has been employed here to estimate the probability of occurrence of one class (it can be control or PD, but we have considered PD class). This method predicts the probability of occurrence of PD by fitting the predictors to a logistic curve using 'logit' logistic function [23] and is given by

$$\text{logit}(P_{PD}) = \ln[P_{PD}(x_1, x_2, \ldots, x_k)/(1 - P_{PD}(x_1, x_2, \ldots, x_k))] = \beta_0 + \beta_1 x_1 + \beta_2 x_2 + \ldots + \beta_k x_k \quad (7)$$

where P_{PD} represents the probability of the subject's outcome to be PD for every observation, β_0 is the constant which represents the intercept in the model, and $\beta = [\beta_1, \beta_2, \ldots, \beta_k]$ are the predictor's regression coefficients. Thus, the probability (risk predictor) of PD for each subject/observation can be expressed as [23]

$$P_{PD} = \frac{1}{1 + e^{-(\beta 0 + \beta i\, xi)}} \quad (8)$$

4 Results and Discussion

This section discusses the PD classification/risk prediction modeling results obtained using SAE along with softmax classifier and MLR, respectively.

4.1 Automatic Classification Based on Softmax Classifier

The proposed method's performance using SAE with softmax classifier is assessed using true positive rate (TPR), true negative rate (TNR), precision (PRE), accuracy (ACC), and F1-score [9, 18, 19]. These values are calculated as follows:

$$TPR = TP/(TP + FN) \quad (9)$$

$$\text{PRE} = \text{TP}/(\text{TP} + \text{FP}) \tag{10}$$

$$\text{TNR} = \text{TN}/(\text{TN} + \text{FP}) \tag{11}$$

$$\text{F1-score} = 2\text{TP}/(2\text{TP} + \text{FP} + \text{FN}) \tag{12}$$

$$\text{ACC} = (\text{TP} + \text{TN})/(\text{TP} + \text{FN} + \text{TN} + \text{FP}) \tag{13}$$

where TP, TN, FP, and FN represent the number of true positive, true negative, false positive, and false negative cases, respectively. In general, TPR measures the ratio of positive cases correctly identified from the total positive cases in the subjects. TNR specifies the correctly classified negative cases. Accuracy specifies the overall performance, i.e. total cases, irrespective of positive and negative classes, which are correctly identified [19]. The dataset used in this study is an imbalanced dataset; therefore, merely calculating the values of TNR, TPR, and ACC is not sufficient due to the possibility of getting biased results [18]. Hence, along with the said performance parameters, PRE and F1-score were also computed. PRE measures the fraction of relevant classes among the retrieved classes and is based on an understanding and measure of relevance. F1-score denotes the test accuracy, and it is calculated as the weighted average of PRE and recall.

All the experiments in this study were performed using Matlab 2017b under Windows environment. Softmax classifier has been used to develop the classification model for identifying the PD subjects from normal subjects, because softmax classifier gives more intuitive output than SVM. The highlights of this study are

(1) The performance of the proposed method was evaluated through TP, TN, FP, FN, and ACC using deep neural network architecture. These performance measures have been calculated for individual SBR features, five most effective biological biomarkers, and various combinations of SBR-biomarkers. They are depicted in Table 2.
(2) Limited features have been used for PD detection. Therefore, there is no need for feature selection methods. Thus, the computational complexity of the proposed method is reduced.
(3) The matched sample size, in terms of age, gender, SBR values, and biological biomarkers (plasma, RNA, CSF, urine, and serum), is significantly large.
(4) To the extent of our knowledge, this is the first instance where the classification/prediction model is developed based on the integration of SBR and biological biomarkers.
(5) As explained later, higher PD detection/risk estimation accuracy is observed using the proposed approach.

4.1.1 Performance Comparison Using the Combination of Different Biomarkers

Higher accuracy of 96.99% in PD detection has been obtained if only SBR values from LC, RC, LP, and RP were considered. This accuracy value is more than the accuracy value obtained using SVM [23]. The maximum accuracy of 100% was achieved by integrating four SBR features and only three biological biomarkers. Further, performance parameters were analyzed by considering different combinations of biological biomarkers with SBR values of LC, RC, LP, and RP.

(a) Analysis based on SBR and individual biological biomarker: In case of the combination of SBR and individual biological biomarkers, a best accuracy of 99.62% was achieved with SBR and plasma.
(b) Analysis based on SBR and biological biomarkers in pair/triplets/quad: Table 2 highlights promising results by using biological biomarkers in pair/triplets/quad along with SBR features. This study proves that SBR values from four regions, when integrated with only one biological biomarker, gives higher accuracy in identifying the PD patients from normal subjects.

Table 2: Performance Parameters of Classification Model Using Softmax Classifier.

Features	TPR	TNR	PRE	ACC	F1-score
SBR (LC, RC, LP, and RP)	93.24	98.44	95.83	96.99	94.52
5 Biological biomarkers	19.59	97.66	76.32	75.94	31.18
SBR + 5 biological biomarkers	100	100	100	**100**	100
SBR with individual biological biomarker					
SBR + CSF	93.20	98.44	95.80	96.80	94.16
SBR + RNA	93.24	98.44	95.83	96.99	94.52
SBR + plasma	98.65	99.68	97.23	**99.62**	99.32
SBR + serum	98.65	98.96	97.33	98.87	97.99
SBR + urine	93.24	97.92	94.52	96.62	93.88
SBR with biological biomarkers in pair					
SBR + serum + urine	90.5	97.6	93.71	95.6	92.10
SBR + plasma + urine	89.9	97.4	93.01	95.3	91.41
SBR + RNA + urine	90.54	97.40	93.06	95.49	91.78
SBR + urine + CSF	90.54	96.41	94.37	95.86	92.41
SBR + serum + CSF	99.32	99.74	99.32	**99.62**	99.32
SBR + RNA + serum	92.57	98.18	95.14	96.62	93.84
SBR + serum + plasma	99.45	99.48	98.67	**99.62**	99.33
SBR + CSF + RNA	99.32	99.48	98.66	99.44	98.99
SBR + CSF + plasma	93.92	97.66	93.92	96.62	93.92
SBR + plasma + RNA	96.62	98.70	96.62	98.12	96.62
SBR with biological biomarkers in triplets					
SBR + CSF + RNA + plasma	100	99.7	99.33	99.8	99.66
SBR + CSF + RNA + serum	90.5	97.4	93.06	95.5	91.78
SBR + CSF + RNA + urine	99.3	99.7	99.32	99.6	99.32
SBR + CSF + plasma + serum	100	100	100	**100**	100
SBR + CSF + plasma + urine	100	100	100	100	100
SBR + CSF + serum + urine	100	100	100	100	100
SBR + RNA + serum + urine	100	99.7	99.33	99.8	99.66
SBR + RNA + serum + plasma	90.5	97.4	93.06	95.5	91.78
SBR + RNA + urine + plasma	91.2	96.9	91.84	95.3	91.53
SBR + serum + urine + plasma	100	100	100	100	100
SBR with biological biomarkers in quad					
SBR + CSF + RNA + plasma + serum	100.00	99.48	98.67	**99.62**	99.33
SBR + CSF + plasma + serum + urine	91.89	97.66	93.79	96.05	92.83
SBR + CSF + plasma + RNA + urine	91.89	97.66	93.79	96.05	92.83
SBR + serum + RNA + plasma + urine	90.54	97.40	93.06	95.49	91.78

4.2 PD Risk Prediction Modeling

Table 3(a) shows the risk estimation PD model using SBR and biological biomarkers. It was observed that the value of 'p' for RC, plasma, and serum was greater than 0.05; hence, these features were not contributing to the results obtained by this model. However, these features are of great importance as discussed in the literature; hence, these features cannot be ignored. To satisfy this constraint, an interaction term (a product of the features) is introduced, instead of working with those individual features.

Table 3(b) reflects the calculated 8-predictor model. Subsequently, it was observed that p-value was less than 0.05 and R-Sq value was significantly high for 8-predictor model. It shows that the logistic model is fitting the data. The obtained model can be expressed as $P_{PD} = \exp(Y')/(1+\exp(Y'))$, where

$$\begin{aligned} Y' = &-20.5 - 0.492 * \text{CSF} + 266.1 * \text{RNA} + 2.690 * \text{urine} - 5.51 * \text{LP} \\ &- 4.494 * \text{RP} + 0.722 * (\text{LC} * \text{RC}) + 0.00802 * \\ &(\text{CSF} * \text{plasma} * \text{serum}) - 19.80 * (\text{RNA} * \text{urine}) \end{aligned} \tag{14}$$

The terms with negative sign in the above equation indicate that PD is negatively correlated with CSF, LP, RP, and the product of RNA and urine.

Table 3: Deviance Table for SBR and Biological Biomarkers

Source	DF	Adj Dev	Adj mean	Chi-square	p-Value	Source	DF	Adj Dev	Adj mean	Chi-square	p-Value
(a)						**(b)**					
CSF (mL)	1	9.075	9.0747	9.07	0.003	CSF (mL)	1	8.981	8.9815	8.98	0.003
RNA (mL)	1	8.921	8.9212	8.92	0.003	RNA (mL)	1	6.158	6.1584	6.16	0.013
Plasma (mL)	1	1.095	1.0946	1.09	0.295	Urine (mL)	1	6.684	6.6838	6.68	0.01
Serum (mL)	1	0.202	0.2025	0.2	0.653	Left putamen	1	50.286	50.2864	50.29	0.00
Urine (mL)	1	7.033	7.0327	7.03	0.008	Right putamen	1	38.128	38.128	38.13	0.00
LP	1	62.078	62.0776	62.08	0.00	LC ∗ RC	1	19.479	19.4788	19.48	0.00
RP	1	56.571	56.571	56.57	0.00	CSF ∗ plasma ∗ serum	1	5.908	5.9077	5.91	0.015
LC	1	21.893	21.8927	21.89	0.00	RNA ∗ urine	1	7.25	7.2499	7.25	0.007
RC	1	0.652	0.652	0.65	0.419						
R-Sq	0.807	R-Sq (Adj)	0.7946	AIC	139.17	R-Sq	0.8305	R-Sq (Adj)	0.8147	AIC	103.42

DF is the degree of freedom that represents the amount of information in the data. Adj Dev is the measure of variation for different components of the model (better explained through R-Sq value). Adj mean measures how much deviance a term or model explains for each DF. Chi-square value determines whether a term or model is associated with response. p-Value specifies the significance level to reject or accept the null hypothesis. Deviance R-Sq and AIC ('Akaike information criterion') are the measures of how well the model fits the data, and relative quality of model. Higher value for deviance R-Sq and smaller value for AIC are preferred to represent the degree of fitness of the data to the model.

4.2.1 Goodness-of-Fit Test

Goodness-of-fit test [23] measures how well the observed data correspond to the fitted model. The Hosmer-Lemeshow test [8] is one of the goodness-of-fit tests used in this study to compare the observed values with the predicted values. This test is based on dividing the samples into groups according to their predicted risks. The Hosmer-Lemeshow test statistics is calculated using the following formula [8]:

$$G^2 = \sum_{j=1}^{n} (O_j - E_j)^2 / [E_j(1 - E_j/n_j)] \approx \chi^2 \tag{15}$$

where χ^2 is called chi-square, and O_j, E_j, and n_j represent the number of observed cases, expected cases, and observations in the jth group, respectively. The output of this test is chi-square value and p-value. The p-value must be high to fit the observations in the model. Table 4 depicts the outcome of Hosmer–Lemeshow goodness-of-fit test. It was observed that the obtained p-value (0.972) was closer to 1 and chi-square value was small with 8 degrees of freedom. The results indicate that the overall model is a fit to the data. This model is helpful in PD risk prediction because the actual output was not different from what was predicted by the risk prediction model.

4.2.2 Predicted Probability's Validation Using MLR

To obtain the accuracy of the identified regression equation, we implemented it on a known training dataset. The quantum to which the predicted probabilities concur with the actual outcome is depicted in the classification table (Table 4). From this table, we can infer that the probability and high PD risk are related to each other.

The overall classification accuracy achieved is 97.37%, indicating high performance accuracy when 8-predictor model is used. The obtained accuracy is higher when compared to the accuracy reported in the literature [23]. Further, to validate the obtained logistic regression model, it was executed on a known test dataset which was different from the training dataset. After the logistic regression, the classification table obtained shows even greater accuracy (Table 5) on the test data. Hence, it is proved that the logistic model fits the data better and can aid the clinicians in diagnosing the PD.

Table 4: Classification Table.

Observed			Predicted
	Normal	PD	% Correct
Normal	143	9	96.62
PD	5	375	97.66
Total N	148	384	97.37
N correct	143	375	
Proportion	0.9662	0.9766	

Sensitivity = 97.66%, specificity = 96.62%, and accuracy = 97.37%.

Table 5: Classification Using Test Dataset.

Observed			Predicted
	Normal	PD	% Correct
Normal	27	1	93.1
PD	2	73	98.6
Total N	29	74	97.1
N correct	27	73	
Proportion	0.931	0.986	

Sensitivity = 98.6%, specificity = 93.1%, and accuracy = 97.1%.

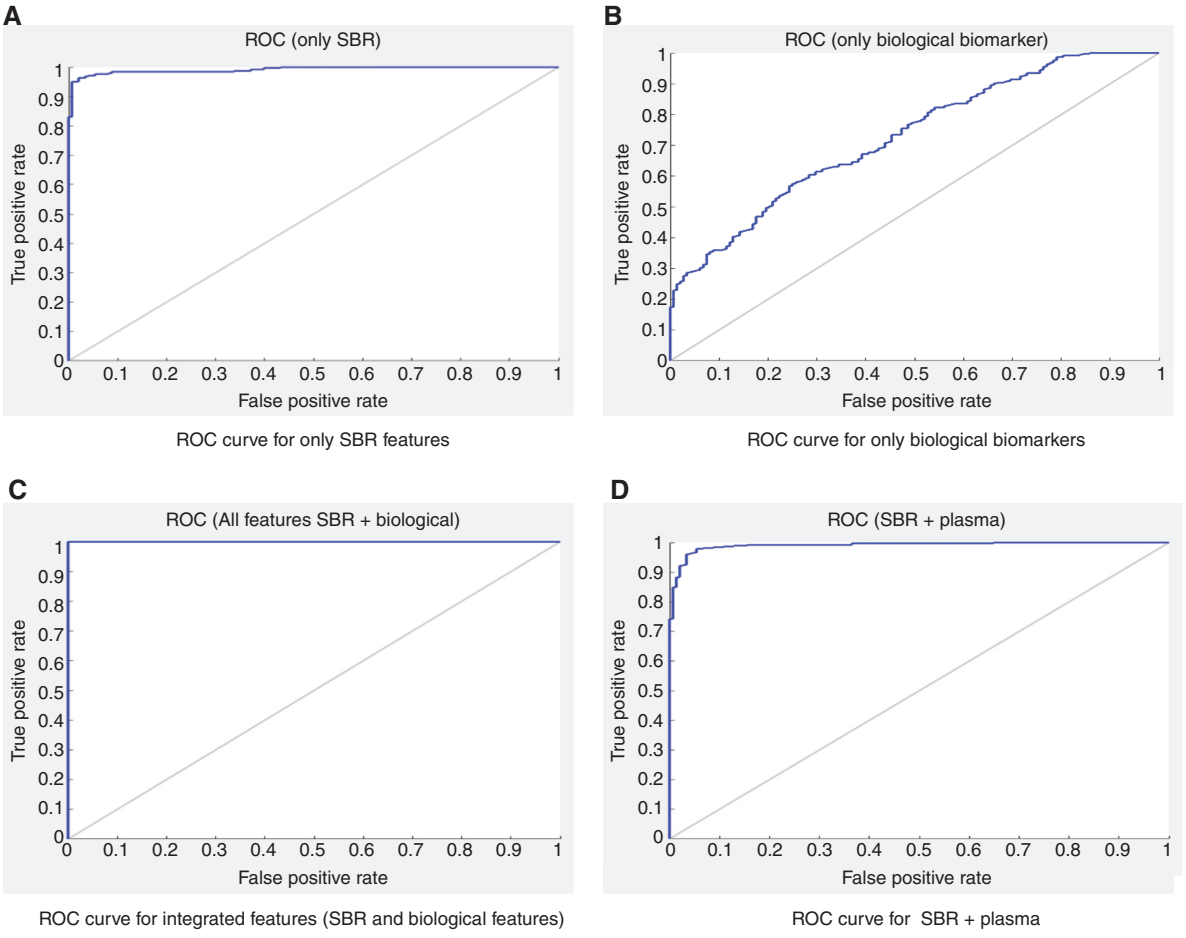

Figure 5: ROC Analysis.

4.2.3 Analysis of Receiver Operating Characteristic Curve

A receiver operating characteristic (ROC) curve [8, 26] is a graph plotted between sensitivity (TPR) and specificity false positive rate (FPR) for a classification procedure due to variation in discrimination threshold. The optimal solution refers to TPR and FPR of 100% and is located in the upper left corner of the curve. If the overall accuracy of the classification procedure is high, then the ROC curve is much closer to the upper left corner.

Figure 5A–D depicts the ROC curve for the proposed method. Figure 5A represents the curve when SBR features alone were used for classifying the PD subjects. The graph highlights the importance of all the four SBR features for PD diagnosis. Considering further accuracy enhancements, some identified biological features have been processed through SAE/softmax classifier. Figure 5B shows the usefulness of biological biomarkers for PD identification. Since both SBR and biological features are contributing towards PD detection, new heterogeneous dataset was created and fed to the SAE/softmax classifier. The obtained results were better than the ones received from individual analysis. ROC in Figure 5C shows the effectiveness of our integrated approach for PD detection. The ROC curve in Figure 5D represents the accuracy, obtained using SBR with plasma, which is also much closer to the upper left corner.

5 Conclusion

This research presented a novel approach to create a prediction/identification model by combining the biological biomarkers with SBR values of only four brain regions, i.e. LP, RP, LC, and RC. The developed model is further validated for its accuracy using a known test dataset.

SBR values from four brain regions and five biological biomarkers, i.e. plasma, serum, urine, RNA, and CSF, of 532 subjects have been obtained from the PPMI database. It has been observed that merely by adding one biological biomarker plasma, PD diagnosis accuracy increases to 99.62%, which is higher than the accuracy reported in the literature. In addition to the PD classification model, PD risk estimation model has also been developed using MLR to showcase that the developed prediction model fits the data well.

Although impressive results have been obtained by the proposed approach, these results need to be validated on a larger dataset if matched features are available. Furthermore, the developed model needs to be validated for the 'scans without evidence for the dopaminergic deficit' subjects.

Acknowledgment: The authors thank PPMI-a, public-private partnership funded by Michael J. Fox Foundation, for providing data for this research.

Bibliography

[1] D. Aarsland, K. Andersen, J. P. Larsen, A. Lolk, H. Nielsen and P. Kragh–Sørensen, Risk of dementia in Parkinson's disease: a community-based, prospective study, *Neurology* **56** (2001), 730–736.

[2] Y. Bengio, Learning deep architectures for AI, *Found. Trends Mach. Learn.* **2** (2009), 1–127.

[3] J. Booij, G. Tissingh, G. J. Boer, J. D. Speelman, J. C. Stoof, A. G. Janssen, E. C. Wolters and E. A. Van Royen, [123I] FP-CIT SPECT shows a pronounced decline of striatal dopamine transporter labelling in early and advanced Parkinson's disease, *J. Neurol. Neurosurg. Psychiatry* **62** (1997), 133–140.

[4] L. M. Chahine, M. B. Stern and A. Chen-Plotkin, Blood-based biomarkers for Parkinson's disease, *Parkinsonism Relat. D.* **20** (2014), S99–S103.

[5] J. L. Cummings, C. Henchcliffe, S. Schaier, T. Simuni, A. Waxman and P. Kemp, The role of dopaminergic imaging in patients with symptoms of dopaminergic system neurodegeneration, *Brain* **134** (2011), 3146–3166.

[6] H. Greenspan, B. Van Ginneken and R. M. Summers, Guest editorial deep learning in medical imaging: overview and future promise of an exciting new technique, *IEEE Trans. Med. Imaging* **35** (2016), 1153–1159.

[7] J. B. Heaton, N. G. Polson and J. H. Witte, Deep learning for finance: deep portfolios, *Appl. Stoch. Models Bus. Ind.* **33** (2017), 3–12.

[8] D. W. Hosmer and S. Lemeshow, *Applied Logistic Regression*, 2nd ed., Wiley, New York, 2000.

[9] V. J. Kadam and S. M. Jadhav, Feature ensemble learning based on sparse autoencoders for diagnosis of Parkinson's disease, in: *Computing, Communication and Signal Processing*, pp. 567–581, Springer, Singapore, 2019.

[10] S. J. Kish, K. Shannak and O. Hornykiewicz, Uneven pattern of dopamine loss in the striatum of patients with idiopathic Parkinson's disease, *New Engl. J. Med.* **318** (1988), 876–880.

[11] A. Krizhevsky and G. E. Hinton, Using very deep autoencoders for content-based image retrieval, in: *European Symposium on Artificial Neural Networks, Computational Intelligence and Machine Learning (ESANN)*, pp. 489–494, Bruges, Belgium, 2011.

[12] A. Krizhevsky, I. Sutskever and G. E. Hinton, Imagenet classification with deep convolutional neural networks, *Adv. Neural Inf. Process. Syst.* **25** (2012), 1097–1105.

[13] Q. V. Le, Building high-level features using large scale unsupervised learning, in: *IEEE International Conference on Acoustics, Speech and Signal Processing (ICASSP)*, pp. 8595–8598, IEEE, Vancouver, BC, Canada, 2013.

[14] F. J. Martinez Murcia, J. M. Górriz, J. Ramírez, M. Moreno Caballero and M. Gómez Río, Parametrization of textural patterns in ^{123}I-ioflupane imaging for the automatic detection of Parkinsonism, *Med. Phys.* **41** (2014), 012502.

[15] F. J. Martinez-Murcia, A. Ortiz, J. M. Górriz, J. Ramírez, F. Segovia, D. Salas-Gonzalez, D. Castillo-Barnes and I. A. Illán, A 3D convolutional neural network approach for the diagnosis of Parkinson's disease, in: *International Work-Conference on the Interplay between Natural and Artificial Computation* 2017, pp. 324–333, Springer, Cham, 2017.

[16] F. J. Martinez-Murcia, A. Ortiz, J. M. Górriz, J. Ramírez, D. Castillo-Barnes, D. Salas-Gonzalez and F. Segovia, Deep convolutional autoencoders vs PCA in a highly-unbalanced Parkinson's disease dataset: a DaTSCAN study, in: *The 13th International Conference on Soft Computing Models in Industrial and Environmental Applications*, pp. 47–56, Springer, Cham, 2018.

[17] F. C. Morabito, M. Campolo, N. Mammone, M. Versaci, S. Franceschetti, F. Tagliavini, V. Sofia, D. Fatuzzo, A. Gambardella, A. Labate and L. Mumoli, Deep learning representation from electroencephalography of early-stage Creutzfeldt-Jakob disease and features for differentiation from rapidly progressive dementia, *Int. J. Neural Syst.* **27** (2017), 1650039.

[18] G. H. Nguyen, A. Bouzerdoum and S. L. Phung, Learning pattern classification tasks with imbalanced data sets, in: P. Yin, ed., *Pattern Recognition*, pp. 193–208, InTech, Rijeka, Croatia, 2009.

[19] G. Orru, W. Pettersson-Yeo, A. F. Marquand, G. Sartori and A. Mechelli, Using support vector machine to identify imaging biomarkers of neurological and psychiatric disease: a critical review, *Neurosci. Biobehav. Rev.* **36** (2012), 1140–1152.

[20] A. Ortiz, J. Munilla, J. M. Gorriz and J. Ramirez, Ensembles of deep learning architectures for the early diagnosis of the Alzheimer's disease, *Int. J. Neural Syst.* **26** (2016), 1650025.
[21] G. Pahuja and T. N. Nagabhushan, Statistical approach towards Parkinson's disease progression, *J. Parkinson Dis. Alzheimer Dis.* **3** (2016), 6.
[22] S. M. Plis, D. R. Hjelm, R. Salakhutdinov, E. A. Allen, H. J. Bockholt, J. D. Long, H. J. Johnson, J. S. Paulsen, J. A. Turner and V. D. Calhoun, Deep learning for neuroimaging: a validation study, *Front. Neurosci.* **8** (2014), 229.
[23] R. Prashanth, S. D. Roy, P. K. Mandal and S. Ghosh, Automatic classification and prediction models for early Parkinson's disease diagnosis from SPECT imaging, *Expert Syst. Appl.* **41** (2014), 3333–3342.
[24] J. Schmidhuber, Deep learning in neural networks: an overview, *Neural Networks* **61** (2015), 85–117.
[25] S. T. Schwarz, T. Rittman, V. Gontu, P. S. Morgan, N. Bajaj and D. P. Auer, T1-weighted MRI shows stage dependent substantia nigra signal loss in Parkinson's disease, *Movement Disord.* **26** (2011), 1633–1638.
[26] F. Segovia, J. M. Gorriz, J. Ramirez, I. Alvarez, J. M. Jimenez-Hoyuela and S. J. Ortega, Improved Parkinsonism diagnosis using a partial least squares based approach, *Med. Phys.* **39** (2012), 4395–4403.
[27] K. D. Seifert and J. I. Wiener, The impact of DaTscan on the diagnosis and management of movement disorders: a retrospective study, *Am. J. Neurodegener. Dis.* **2** (2013), 29.
[28] A. Shtilbans and C. Henchcliffe, Biomarkers in Parkinson's disease: an update, *Curr. Opin. Neurol.* **25** (2012), 460–465.
[29] R. Socher, B. Huval, B. Bath, C. D. Manning and A. Y. Ng, Convolutional-recursive deep learning for 3D object classification, *Adv. Neural Inf. Process. Syst.* **25** (2012), 656–664.
[30] H. I. Suk and D. Shen, Deep learning-based feature representation for AD/MCI classification, in: *International Conference on Medical Image Computing and Computer-Assisted Intervention*, pp. 583–590, Springer, Berlin, Heidelberg, 2013.
[31] S. Takaya, N. Sawamoto, T. Okada, G. Okubo, S. Nishida, K. Togashi, H. Fukuyama and R. Takahashi, Differential diagnosis of Parkinsonian syndromes using dopamine transporter and perfusion SPECT, *Parkinsonism Relat. D.* **47** (2018), 15–21.
[32] T. Tokuda, S. A. Salem, D. Allsop, T. Mizuno, M. Nakagawa, M. M. Qureshi, J. J. Locascio, M. G. Schlossmacher and O. M. El-Agnaf, Decreased α-synuclein in cerebrospinal fluid of aged individuals and subjects with Parkinson's disease, *Biochem. Biophys. Res. Commun.* **349** (2006), 162–166.
[33] E. Tolosa, T. V. Borght, E. Moreno and DaTSCAN Clinically Uncertain Parkinsonian Syndromes Study Group, Accuracy of DaTSCAN (123I-ioflupane) SPECT in diagnosis of patients with clinically uncertain Parkinsonism: 2-year follow-up of an open-label study, *Movement Disord.* **22** (2007), 2346–2351.
[34] K. Zeng, J. Yu, R. Wang, C. Li and D. Tao, Coupled deep auto-encoder for single image super-resolution, *IEEE Trans. Cybern.* **47** (2017), 27–37.
[35] Y. N. Zhang, Can a smartphone diagnose Parkinson disease? A deep neural network method and telediagnosis system implementation, *Parkinsons Dis.* **2017** (2017). Article ID: 6209703, 11 pages.
[36] G. Zubal, G. Wisniewski, K. Marek and J. Seibyl, Automated program for analyzing striatal uptake of DaTSCAN SPECT images in humans suspected of Parkinson's disease, *J. Nucl. Med.* **52** (2011), 2098–2098.

Bionotes

Gunjan Pahuja
Department of Computer Science and Engineering, JSS Academy of Technical Education, Noida 201301, India; and
Dr. A. P. J. Abdul Kalam Technical University, Lucknow, India

Gunjan Pahuja received her M. Tech. degree from Guru Jambheshwar University of Science and Technology, Hisar, in 2006. Currently, she is working towards a Ph.D. degree in the Department of Computer Science and Engineering from Dr. A. P. J. Abdul Kalam University, Lucknow. Her research focuses on Machine Learning and Medical Image Processing.

T. N. Nagabhushan
Department of Information Science and Engineering, Sri Jayachamarajendra College of Engineering,
Mysuru 570006, India

T. N. Nagabhushan received his Master's and Ph.D. degrees in Electrical Engineering from Indian Institute of Science, Bangalore, in the years 1989 and 1996, respectively. He has over 32 years of experience in teaching, research, and industry besides holding the position of principal. His main area of focus is machine learning, development of new tools for supervised learning, and applications to image processing. He is a member of ISTE and CSI.

Bhanu Prasad
Department of Computer and Information Sciences, Florida A&M University, Tallahassee, FL 32307, USA
bhanu.prasad@famu.edu

Bhanu Prasad received his Master of Technology and Ph.D. degrees, both in Computer Science, from Andhra University and Indian Institute of Technology Madras, respectively. His current research interests include Artificial Intelligence and Software Engineering.